Computers & Industrial Engineering 169 (2022) 108251

Contents lists available at ScienceDirect

Computers & Industrial Engineering

journal homepage: www.elsevier.com/locate/caie

Performance optimization of hard rock tunnel boring machine using multi-objective evolutionary algorithm

Zhun Fan [a,c,d,e], Zehao Zheng [a,b], Biao Xu [a,f,*], Wenji Li [a], Yonggang Zhang [f], Zhifeng Hao [a]

[a] Department of Electronic Engineering, Shantou University, Shantou 515063, China
[b] Department of Physics and Electronic Engineering, Hanshan Normal University, Chaozhou 521041, China
[c] Key Lab of Digital Signal and Image Processing of Guangdong Province, Shantou University, Shantou 515063, China
[d] Key Laboratory of Intelligent Manufacturing Technology (Shantou University), Ministry of Education, Shantou 515063, China
[e] State Key Lab of Digital Manufacturing Equipment & Technology, Huazhong University of Science and Technology, Wuhan 430074, China
[f] Key Laboratory of Symbolic Computation and Knowledge Engineering of Ministry of Education, Jilin University, Changchun 130012, China

ARTICLE INFO

Keywords:
Constrained multi-objective optimization
TBM performance optimization
TBM modeling

ABSTRACT

The hard rock Tunnel Boring Machine (TBM) is a complex engineering equipment coupled with multiple subsystems for underground tunnel excavation in complex geological environments. Resetting the operational and structural parameters of TBM according to different geological conditions usually requires engineers to spend a lot of time dealing with the interaction between various subsystems, which is a tedious and time-consuming job. To facilitate setting the operational and structural parameters of TBM, we present a constrained multi-objective optimization model and its solving method in this paper. To be specific, three performance indices, i.e. minimizing the system construction period, construction energy consumption and construction cost of TBM, are firstly considered as the three objectives in the proposed model. Secondly, two push and pull search (PPS) based algorithms, including PPS-MOEA/D and PPS-KnEA, are suggested to solve the formulated constrained multi-objective optimization problem. Finally, to verify the performance of the developed method, the presented method is compared with several popular constrained multi-objective evolutionary algorithms by tackling the established optimization model. The experimental results reveal that the presented method has the best performance among the comparison algorithms, and the overall performance of the algorithm with PPS is better than other algorithms without PPS, which indicates the superiority of PPS framework in solving practical optimization problems.

1. Introduction

TBM is a large underground engineering machine with tightly coupled subsystems. It is widely used in the construction of water conservancy, subway, and other infrastructure due to its good construction safety, high tunneling efficiency and environmental protection characteristics (Yagiz & Karahan, 2011; Sun, Wang, Wang, Zhang, & Song, 2016; Liao, Chen, & Yao, 2017; Ren, Shen, Zhou, & Chai, 2018a). However, it also has problems such as long construction period, high cost, and large energy consumption, especially the expensive hard rock TBM. In order to find feasible and mature TBM operational and structural parameters, engineers usually deal with the interaction between different subsystems according to engineering experience, which not only involves a lot of repetitive work but also affects the selection of the best operational and structural parameters. Moreover, different subsystems of TBM belong to different disciplines, including geotechnical, mechanical, electromagnetic, information, hydraulic, and other disciplines. The tight coupling of a large number of subsystems and disciplines brings great challenges for engineers in setting TBM system parameters.

Researchers have built many mathematical models of TBM to help engineers understand the relationships between each subsystem and provide a basis for regulating operational parameters. For example, Wijk (1992) used the uniaxial compressive strength of the rock and the cerchar abrasivity index of the rock to propose the wear equation of the TBM's disc cutter and simulated the relationships between the structure of the disc cutter and other subsystems. Roxborough and Phillips (1975) first attempted to determine the fundamental relationships between the

* Corresponding author at: Department of Electronic Engineering, Shantou University, Shantou 515063, China
E-mail address: xubiao@stu.edu.cn (B. Xu).

https://doi.org/10.1016/j.cie.2022.108251
Received 14 July 2021; Received in revised form 20 April 2022; Accepted 14 May 2022
Available online 20 May 2022

normal forces and rolling forces acting on the rock surface and the uniaxial compressive strength, disc diameter, and penetration of the rock. To describe the force on the cutter more precisely, Ozdemir (1977) established a TBM model taking into account the spacing of the cutter. He observed that there was an optimal spacing to penetration ratio. Rostami and Ozdemir (1993) established a new theoretical/empirical Colorado School of Mines model for TBM, which can also be used to optimize the design of disc cutter and calculate the penetration rate of TBM under given geological conditions. Rostami (1997) developed the Colorado School of Mines model and establishing more precisely the relationships between the pressure on the disc cutter and various parameters. Yagiz (2003) analyzed and evaluated the impact of rock fracture and brittleness on TBM performance, and modified the Colorado School of Mines model.

To make the mathematical model reflect the performance of TBM more accurately and obtain the optimal operation and structural parameters, artificial intelligence technology has been widely used in the optimization and construction of TBM model in the past two decades (Yagiz & Karahan, 2011; Armaghani, Mohamad, Narayanasamy, Narita, & Yagiz, 2017; Yagiz & Karahan, 2015). Specifically, Benardos and Kaliampakos (2004) built the tunneling speed model by using Artificial Neural Network. Grima, Bruines, and Verhoef (2000) found that TBM modeling with neuro-fuzzy method had more accurate results than traditional modeling methods. Moreover, Sun, Wang, Shi, Wang, and Song (2018);Wang, Yuan, Mu, Sun, and Song (2019) employed genetic algorithm (GA) to find the optimal control and structural parameters, and studied the influence of different TBM prediction models on the minimum construction period of tunnel engineering. Armaghani, Faradonbeh, Momeni, Fahimifar, and Tahir (2018) used the gene expression programming(GEP) to build an equation model of TBM to estimate the performance of TBM, and found that the GEP equation was superior to the multiple regression equation. Wang and Wang (2020) transformed the multi-objective problem of TBM into a single objective problem, and took the single objective function as a linear combination of multiple objective functions. For the past few years, combining of deep learning and evolutionary algorithm are also applied on TBM. For example, Yagiz and Karahan (2011) combined artificial neural network and particle swarm optimization to predict the advance speed of granite tunneling machines in different weathered zones.

Although a lot of work has been done on the optimization of the TBM performance, most of the work focused on the construction of TBM model and the single-objective optimization of performance indices. Wang and Wang (2020) presented several crucial performances of TBM during the excavating, and employed them as objective function in later formulation of multi-objective optimization problem for TBM control. However, they converted the established multi-objective optimization problem into single-objective optimization problem with setting well-matched weighted factors and provided only one solution. As a matter of fact, TBM model includes many performance indices, such as construction period, construction energy consumption, and construction cost. When any performance index decreases by changing subsystem operational parameters, it may lead to the increase of other performance indices. It is not appropriate to consider only one objective for optimization. It must be balanced between low cost, low construction period, and low energy consumption. Therefore, multi-objective optimization model for TBM is very necessary. As far as we know, there are a few researches on multi-objective optimization of TBM models using constrained multi-objective evolutionary algorithms (CMOEAs), so it is urgent to fill this gap.

In addition, the optimization of TBM is often involved in many constraints, such as constraints on the power output from the hydraulic thrust system of the cutterhead, constraints on the power output from the cutter head driving system, geometric constraints on the disc cutter design(Wijk, 1992), performance requirements, etc. The TBM performance optimization problem can be summarized as a constrained multi-objective optimization problem (CMOP). Without loss of generality, a CMOP can be defined as follows:

$$\begin{cases} \text{minimize} & \mathbf{F}(\mathbf{x}) = (f_1(\mathbf{x}), \ldots, f_m(\mathbf{x}))^T \\ \text{subject to} & g_i(\mathbf{x}) \geqslant 0, i = 1, \ldots, q \\ & h_j(\mathbf{x}) = 0, j = 1, \ldots, p \\ & \mathbf{x} \in \mathbb{R}^n \end{cases} \tag{1}$$

where $F(\mathbf{x})$ is an m-dimensional objective vector, and $F(\mathbf{x}) \in \mathbb{R}^m$. $g_i(\mathbf{x}) \geqslant 0$ refers to inequality constraints, and q means the number of inequality constraints. $h_j(\mathbf{x}) = 0$ is an equality constraint, and p represents the number of equality constraints. $\mathbf{x} \in \mathbb{R}^n$ refers to an n-dimensional decision vector.

A feasible solution set, $FS = \{\phi(x) = 0, x \in \mathbb{R}^n\}$, is constituted by all feasible solutions. Given a solution $\mathbf{x}^* \in FS$, if there is no any other solution $\overline{\mathbf{x}}^* \in FS$ satisfying $f_i(\overline{\mathbf{x}}^*) \leqslant f_i(\mathbf{x}^*)(i \in \{1, \ldots, m\}), \mathbf{x}^*$ is called a Pareto optimal solution. All Pareto optimal solutions constitute a Pareto set (PS). The set of the mapping vectors of PS in the objective space is called a Pareto front (PF), which is defined as $PF = \{F(\mathbf{x}) | \mathbf{x} \in PS\}$.

In recent years, a series of CMOEAs are proposed to tackle the CMOPs. CMOEAs mainly consist of two parts: (1) multi-objective optimization evolutionary algorithm; (2) constraint processing mechanism. Due to objectives are always in conflict with each other, CMOEAs not only need to maintain a balance between convergence and diversity of working population, but also need to maintain a balance between objective minimization and constraint satisfaction, so as to find an optimal set of compromise solutions.

Existing CMOEAs fall into three different types according to their selection mechanism. The first type is a domination-based CMOEA, such as NSGA-II-CDP (Deb, Pratap, Agarwal, & Meyarivan, 2002), which uses a non-dominant sorting method to select solutions to the next generation. The second is decomposition based CMOEA. A typical example of this type is MOEA/D-CDP (Zhang & Li, 2007), which decomposes a CMOP into a number of constrained single-objective optimization problems, each of which is solved in a collaborative manner. Finally, index-based CMOEA, such as KnEA (Zhang, Tian, & Jin, 2015; Tian, Zhang, Xiao, Zhang, & Jin, 2021), used hypervolume metrics to improve the convergence and diversity of the algorithm. In addition, for multi- and many-objective optimization problems, the compromise among the optimization objectives is different for each Pareto-optimal solution. Hence, the solution that has the best compromise among the objectives should satisfy the decision-maker's constraints and preferences (Rao, 2007). Rao and Lakshmi (2021a, 2021b) presents a R-method to selecting the best solution in the problems via ranking of Pareto-optimal solutions. First, the level assigned to the objectives and the alternative solutions that relative to each objective are converted into appropriate weights. These weights are used to calculate the final comprehensive score of the alternative solutions. Then the final ranking of alternative solutions is done based on the composite scores. At last, the experiments reveal that the proposed method is comparatively easier, more logical, and can be used for choosing the best compromise solution in multi- and many-objective optimization problems.

In this paper, we formulate a TBM performance optimization as a CMOP. The modeled CMOP contains a number of inequality constrains. for a practical problem, it usually has small and narrow feasible regions. Moreover, the infeasible regions will block the way of the searching population towards the PF. Hence, it is very difficult to solve a CMOP, due to three types of difficulty, convergence difficulty, diversity difficulty, and feasibility difficulty (Fan et al., 2019a) exist in the problem. Recently, a kind of push and pull search (PPS) framework was proposed for solving CMOPs by Fan et al. (2019c, 2019b). The PPS framework is appropriate for the CMOP with small and narrow feasible regions. Two PPS-based algorithms, including PPS-MOEA/D and PPS-KnEA (embedding Finding knee points method in the PPS framework), are suggested to solve the formulated CMOP. The main contributions of the paper are as follows:

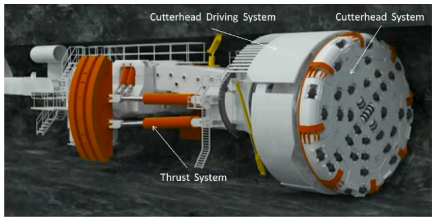

Fig. 1. The whole structure of TBM(Sun et al., 2016).

1. The mathematical model of TBM was established and the performance of TBM was optimized into CMOP.
2. A PPS-based algorithm called PPS-KnEA which is also a knee point driven CMOEA is proposed. In the infeasible solution of the current population, the knee points preference is an approximation of the very large hypervolume preference, and the knee points are pushed to the feasible region from the infeasible region with the help of PPS framework, thus improving their diversity and convergence performance in CMOP.
3. Within the PPS-KnEA, a new constraint multi-objective optimization strategy using knee point driven and improved epsilon constraint handling mechanism are proposed. In this strategy, the local knee points of the non-dominated fronts in the population is first locating. Then, the improved epsilon constraint handling mechanism is employed to control the constraint violation values of each generation dynamically. If the constraint violation values of the infeasible solutions are less than or equal to a predefined threshold value, the knee points in the neighborhood are preferentially selected to accelerate the convergence and promote diversity.

The rest of this paper is organized as follows. In Section 2, the modeling of the TBM is detailed, with its optimization formulated as a CMOP. In Section 3, a modified PPS-based algorithm called PPS-KnEA is proposed. Section 4 designs experiments to compare PPS-MOEAD and PPS-KnEA with four CMOEAs, including CM2M, MOEA/D-CDP, KnEA, and NSGA-II-CDP. Finally, conclusions and some future research directions are summarized in Section 5.

2. Problem formulation

2.1. Model of hard rock TBM

In hard rock TBM tunnel construction, it is necessary to reset the operation parameters and structure design parameters of the disc cutter according to the different geological conditions. That is a tedious and time-consuming task, especially in complicated geological conditions of the construction environment, which need frequent to resetting the system parameters to adapt the changing of rock types. Furthermore, the main system of a TBM can be divided into the following three subsystems: the thrust system, the cutter head driving system and the cutter head system as shown in Fig. 1. The variation of the parameters in a subsystem will affect the parameters of the other subsystems. That is, the 3 subsystems interact and constrain each other to form a tightly coupled mechanical system (Rostami, 2016; Liu et al., 2016b; Home, 2016).

2.1.1. Thrust system

The thrust system provides a stable and reliable power source for the rock breaking progress of TBM, which has an important impact on the construction period, energy consumption and cost. The thrust system pushes the disc cutter onto the rock surface and acts a normal force F_n to squeeze and penetrate the rock, as shown in Fig. 2(a). The projected area of the disc cutter acting on the rock surface is trapezoid A, and the area of the trapezoid is provided as follows. ”

$$A = \frac{1}{2}\left[\left(w + w + 2\delta tan\alpha\right)\sqrt{r^2 - (r-\delta)^2}\right] \tag{2}$$

where w(m) is the disc cutter wear flat, r(m) means the radius of the cutter, α(°) refers to the cutter edge angle, and δ(m) means the penetration depth. According to Wijk (1992)'s rock pressure equation, it can be known that the thrust acting on each disc cutter is f_n:

$$f_n = 3\sigma_c A \tag{3}$$

where σ_c (Pa) is the UCS of the rock, assuming that the thrust acting on each cutter is the same, then the total thrust needed to break the rock on the cutter head is F_n:

$$F_n = N_T f_n \tag{4}$$

where N_T is the total number of the disc cutter, by combining Eqs. ()() (2)–(4), we obtain that the total thrust force of the thrust system applied

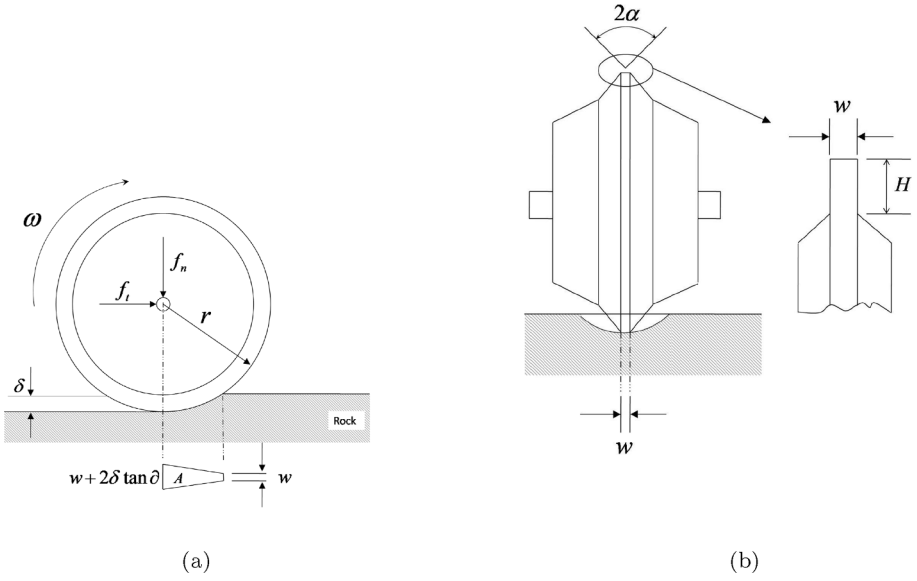

Fig. 2. The structure of the constant wear flat disc cutter.

Table 1
Nomenclature.

w	the disc cutter wear flat (m)	r	the radius of the cutter(m)
α	the cutter edge angle (°)	δ	the penetration depth (m)
F_n	thrust force of the thrust system (N)	f_n	the thrust acting on one disc cutter (°)
A	the projected area (m^2)	P_F	the total power on the thrust system (W)
ω	the rotating speed (rd/min)	α	the cutter edge angle (°)
f_t	tangential force of one disc cutter (N)	T_t	the total torque (Nm)
N_T	the total number of the disc cutter	η	the friction coefficient
σ_{PLT}	the Point Load Test index for tensile rock strength(Pa)	P_T	the total power on the cutter-head driving system (W)
H	the wear height for constant wear flat tool(m)	φ	the Cutter wear coefficient (Pa/m^2)
D	the diameter of the cutterhead (m)	CAI	Cerchar abrasivity index
L_o	the length of each ring(m)	L_T	the total length of the tunnel (m)
t_n	the normal excavation time (h)	t_d	the down time (h)
t_{cha}	the time of replacing the cutter (h)	t_{mai}	the maintenance time (h)
C_f	the cutter-life of the disc cutter (m)	λ	the proportionality constant
E	the construction energy consumption (m)	L_z	the total rolling length of all cutters (m)
N_c	the number of the changed cutters	M	the TBM capital cost ($/h)
C_t	the tools cost ($)	C	the construction cost ($)

to the cutter head is F_n:

$$F_n = 3N_T\sigma_c\left(w+\delta tan\alpha\right)\sqrt{2r\delta-\delta^2} \tag{5}$$

Therefore, the total power on the thrust system is:

$$P_F = \frac{F_n\delta\omega}{60} \tag{6}$$

where ω(rd/min) is the rotating speed, the corresponding notations are explained in Table 1.

2.1.2. Cutterhead driving system

The cutterhead hydraulic driving system provides a reliable and stable torque T_t for the rotation of the cutterhead. The rotation of the cutterhead provides a tangential force f_t for the disc cutter which is attached to the cutterhead (Wang, Kang, Zhao, & Zhang, 2015; Zhang, Huang, Huang, Cai, & Kang, 2013). From Wijk (1992)'s work, its tangential force equation can be obtained as follows:

$$f_t = 3\sigma_c\delta\left(w+\frac{2}{3}\delta tan\alpha\right) \tag{7}$$

According to the definition of friction, the friction coefficient is assumed to be η, then:

$$\eta = \frac{f_t}{f_n} \tag{8}$$

Then the total torque on the cutterhead is:

$$T_t = \eta \quad F_nD\frac{N_T+1}{4N_T} \tag{9}$$

By combining (5), (7), (8) and (9), we can get the total torque applied to the cutting head as follows:

$$T_t = \frac{N_T+1}{4N_T}F_nD\frac{\delta\left(w+\frac{2}{3}\delta tan\alpha\right)}{\left(w+\delta tan\alpha\right)\sqrt{2r\delta-\delta^2}} \tag{10}$$

where D (m) is the diameter of the cutterhead, So the total power on the cutter-head driving system is:

$$P_T = \frac{2\pi\omega T_t}{60} \tag{11}$$

2.1.3. Cutterhead system

The disc cutter attached to the cutterhead system is a system in direct contact with the rock (Ren, Shen, Arulrajah, & Cheng, 2018b). It is necessary to design different disc cutter structures according to different geological parameters and cooperate with appropriate operational parameters, so as to maximize the cutter-life of the disc cutter and save construction cost without affecting the construction period and energy consumption(Armaghani, Koopialipoor, Marto, & Yagiz, 2019; Singh, 2014; Rostami, 2008). Here, Wijk (1992)'s cutter-life model is adopted as follows:

$$C_f = \frac{2rw^3\varphi cot\frac{\alpha}{2}}{F_n(CAI)^2\sqrt{\sigma_c\sigma_{PLT}}} \tag{12}$$

where $\varphi(Pa/m^2)$ means the cutter wear coefficient, σ_{PLT}(Pa) refers to the point load test index for tensile rock strength.

2.2. Optimization variables

Six control variables are considered in the optimization problem, which are defined as: $x = [H,w,\delta,\omega,r,\alpha]$. H and $w$are the wear height and flat of the disc cutter respectively, and $\delta$is the penetration depth. α is the cutter edge angle, ω presents the rotary speed, r refers to the disc cutter radius. In addition, the ranges of design variables are provided in Table 2, the values for a set of the constant parameters are provided in Table 3.

Table 2
The ranges of design variables.

Variables	Range	Units	Original design
H	[0.5,20]	mm	0.5
w	[2,20]	mm	2
δ	[1,20]	mm	5
α	[30,120]	°	80
ω	[0.5, 10]	rd/min	6
r	[100, 300]	mm	200

Table 3
The values of the related parameters.

Parameter	value	Units
D	10	m
L_o	1	m
φ	1.7×10^{25}	Pa^2/m
σ_c	1.3×10^{8}	Pa
σ_{PLT}	7.5×10^{6}	Pa
CAI	2.5	
L_T	10000	m
N_T	40	one

2.3. Objectives

In the tunnel construction project of TBM, the construction period, energy consumption and cost are the three performance indices that need to be considered. The optimization of TBM performance is a multi-objective optimization problem, so we consider minimizing the construction period, energy consumption and cost.

2.3.1. Minimize construction period

The excavation period of the tunnel is mainly divided into normal excavation time (t_n), and down time (t_d) which mainly includes the time of replacing the cutter (t_{cha}) and maintenance time ($t_{mai} = \varsigma * t_n$), where

ς is the coefficient, so the total construction period is (Sun et al. (2018)):

$$t = t_n + t_d = t_n + t_{cha} + \varsigma * t_n \tag{13}$$

where

$$\begin{cases} t_n = \dfrac{L_T}{60\delta\omega} \\ t_{cha} = t_{chas} floor\left(\dfrac{L_z}{C_f}\right) \\ L_z = \dfrac{\pi D(N_T+1)L_T}{2\delta} \end{cases} \tag{14}$$

L_T is the total length of the tunnel, L_z presents the total rolling length of all cutters, t_{chas} refers to the changing time of each cutter. Thus, the first objective function can be written as follows:

$$f_1 = min(t) \tag{15}$$

2.3.2. Minimize construction energy consumption

In TBM tunnel engineering, in order to ensure engineering energy saving, we reduce the construction energy consumption of each ring of the tunnel to the minimum. In this study, the construction energy consumption mainly includes hydraulic thrust system and tool head torque system. The construction energy consumption can be calculated by the following formula.

$$E = \left(P_F + P_T\right)\frac{L_T}{60\delta\omega} \tag{16}$$

Thus, the second objective function can be written as follows:

$$f_2 = min(E) \tag{17}$$

2.3.3. Minimize construction cost

In the TBM tunnel project, in order to reduce the cost of the project, we minimize the construction cost of each ring of the tunnel. In this study, the cost of the project mainly includes the rent of TBM and the expenditure of the disc cutter. The construction cost of the tunnel can be calculated by the following formula.

$$C = \frac{M_T L_T}{60\delta H\omega} + \left(N_T + N_c\right)C_t \tag{18}$$

where N_c is the number of the changed cutters, M_T means the TBM capital cost, C_t refers the tools cost. Thus, the third objective function can be written as follows:

$$f_3 = min(C) \tag{19}$$

2.4. Constraints

The constraints of TBM mainly include the design of the disc cutter and performance constraints of the thrust system, cutterhead driving system. Therefore, there are the following six constraints:

$$\lambda = \frac{H}{w} \tag{20}$$

Equation.(20) represents the constraints on the design of the disc cutter. H is the wear height for constant wear flat disc cutter, and λ is the proportionality constant. Cutter wear flat w and cutter wear height H are two mutually constrained variables. The smaller the cutter wear flat is, the sharper the cutter is, the higher the driving speed is. However, it is easy to be damaged, the cutterlife of the cutter is shorter, increasing the cost of the cutter. In order to reduce tool consumption, disc cutter wear height H should be as large as possible, but wear plane w must increase with the increasing of wear height H, to obtain stable cutting performance. Therefore, λ should not be greater than 1.5.

$$1.5 - \lambda \geqslant 0 \tag{21}$$

In order to maintain the performance of the tool and the successful completion of the project, we limit the cutterlife of the tool to within 3000 meters.

$$3000 - C_f \geqslant 0 \tag{22}$$

The torque system consists of a set of hydraulic motors which has a limit to the maximum output torque. Exceeding this limit will easily cause the cutterhead to get stuck, resulting in unnecessary downtime for maintenance, in which case the total torque is less than 5,000 KNm:

$$5 \times 10^6 - T_t \geqslant 0 \tag{23}$$

Similarly, the hydraulic thrust system provides a limit to the thrust of the cutter. In addition to overcoming the ground resistance from penetrating the rock, it also prevents damage to the disc cutter. In general, the total thrust should be less than 15,000 KN:

$$1.5 \times 10^7 - F_n \geqslant 0 \tag{24}$$

In addition, both the Cutterhead driving system and the Thrust system are limited in the output power. Exceeding the mechanical load will make the TBM unable to work normally and even bring potential construction safety hazards. The constraint equations are as follows:

$$4.5 \times 10^6 - P_T \geqslant 0 \tag{25}$$

$$1.2 \times 10^4 - P_F \geqslant 0 \tag{26}$$

In summary, the overall optimization model contains three objectives (minimizing construction period, energy consumption, cost), and six constraints (including the design of the disc cutter, performance constraints of the thrust system and cutter head driving system). The overall optimization model is provided as follows.

$$\begin{cases} \text{minimize} & \mathbf{F}(\mathbf{x}) = (t, E, C)^T \\ \text{subject to} & 1.5 - \lambda \geqslant 0 \\ & 3000 - C_f \geqslant 0 \\ & 5 \times 10^6 - T_t \geqslant 0 \\ & 1.5 \times 10^7 - F_n \geqslant 0 \\ & 4.5 \times 10^6 - P_T \geqslant 0 \\ & 1.2 \times 10^4 - P_F \geqslant 0 \end{cases} \tag{27}$$

3. PPS-KnEA

PPS-KnEA is in principle a knee point driven CMOEA based on PPS framework. The main difference between PPS-KnEA and PPS-MOEA/D is that, in addition to the dominance relationship, the knee point is used as a preferred selection criterion. In the process of environmental selection, PPS-KnEA preferentially selected individuals carrying knee points to improve the diversity of the population. In this section, we describe the main components of PPS-KnEA.

3.1. Definition of knee points

A knee point, B_k, is defined to be the one having the maximum distance from the convex hull of individual minima to the hyperplane S constructed by the extreme points.

$$B_k = arg\max_p \left\{ \left(d\left(p, S\right) \right) \right\} \tag{28}$$

where p is a solution on the PF. $d(p,S)$ denotes the distance from solution p to the hyperplane S: $f_1 + \ldots + f_m = 1$ in a normalized coordinator system(Yu, Jin, & Olhofer, 2020).

In the above definition, an extreme point x in the i-th objective can be described as follows for a given population P: $\forall y \in$ P, $\exists i \in$

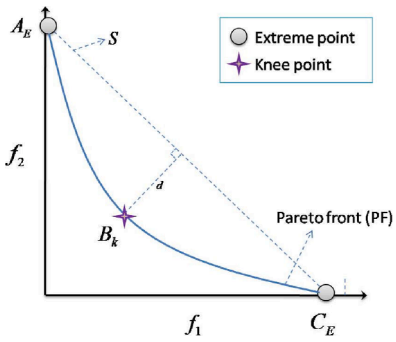

Fig. 3. An illustrative example of the knee point (B_k) of a PF. Solutions A_E and C_E are the extreme points.

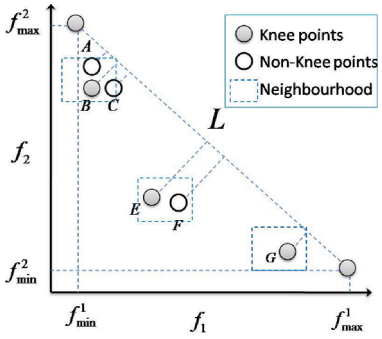

Fig. 4. An illustration for finding knee points for a biobjective minimization problem.

$\{1,\ldots,m\}, x = argmax f_i(y) \wedge \forall j \in \{1,\ldots,i-1,i+1,\ldots,m\}, f_j(x) = min f_j(y)$. In Fig. 3, point B_k is the knee point on the PF, which has the largest distance to the hyperplane constructed by the extreme points, A_E and C_E. Additional definitions of knee points can be found in Qiu, Liu, Zhang, Li, and Cheng (2019), Zhang et al. (2015) and Das (1999).

3.2. Finding knee point method

In the multi-objective optimization of real world problems, a small improvement in one of the objectives would result in a severe degradation of at least one other objectives. Knee points are a subset of the Pareto optimal solution. Hence, when the user has no specific preference for the Pareto solution, knee point is considered the preferred solution. In this work, we adopt the Finding knee point method presented by Zhang Zhang et al. (2015). By looking at Fig. 4, we can see that solution B is a knee point in its neighborhoods denoted by the rectangle in dashed lines, as it has the maximum distance to L among A, B and C inside its neighborhood. From Fig. 4, we can conclude that the knee point in the evolution population has the maximum hypervolume value. Therefore, with guidance of the knee point, the evolution population are able to accelerate convergence and maintain diversity (Zhang et al., 2015; Yu et al., 2020).

For a bi-objective problem, L can be defined by $ax + by + c = 0$, where the parameters can be determined by the two extreme solutions. Then the distance from a solution $A(x_A, y_A)$ to L can be calculated as follows:

$$d\left(A, L\right) = \begin{cases} \dfrac{|ax_A + by_A + c|}{\sqrt{a^2 + b^2}} & \text{if} ax_A + by_A + c \\ -\dfrac{|ax_A + by_A + c|}{\sqrt{a^2 + b^2}} & \text{otherwise} \end{cases} \tag{29}$$

" If the set of mapping vectors in the objective space for the solutions of generation g contains N_g nondominated solutions based on non-dominated sorting, and each set of nondominated soltuions has S_i ($1 \leqslant i \leqslant N_g$) solutions." $1 \leqslant i \leqslant N_g$. The neighborhood of the solutions is defined by the size of the hypercube $R_g^1 \times R_g^2 \times \cdots \times R_g^j \times \cdots \times R_g^M$, where $1 \leqslant j \leqslant M, M$ represent the number of objectives. So, the size of the neighborhood regarding objective j, R_g^j is determined as follows:

$$R_g^j = \left(f_{max_j^g} - f_{min_j^g}\right) \cdot r_g \tag{30}$$

where $f_{max_g^j}$ and $f_{min_g^j}$ represent the maximal and the minimal values of the j-th objective at the g-th generation in set S_i, and r_g is the ratio of the size of the neighborhood to the span of the j-th objective in non-dominated front S_i at generation g, which is updated as follows:

$$r_g = r_{g-1} * e^{-\frac{1-t_{g-1}}{T}/M} \tag{31}$$

where r_{g-1} means the ratio of the size of the neighborhood to the span of the j-th objective of the solutions in S_i at the $(g-1)$-th generation, t_{g-1} refers the ratio of knee points to the number of non-dominated solutions in front i at the $(g-1)$-th generation, and $0 < T < 1$ is a threshold that controls the ratio of knee points in the solution set S_i.

3.3. PPS framework

In CMOPs, the constraints define infeasible regions in the decision space, and have an effect on the PF in the objective space. The influence of infeasible regions on PFs exists in the following three situations. On one hand, infeasible regions may block the way of evolutionary population towards the PF; On the other hand, the unconstrained PF is covered by infeasible regions and all of it is infeasible; Finally, infeasible regions make the original unconstrained PF partially feasible. PPS mainly prefers to focus on the above situations. The PPS framework can be described as the following two stages: push search and pull search. In the stage of push search, the constraints are ignored and the population converges to the unconstrained PF, so that the population can cross the infeasible region without being blocked. If the change of the population fitness within several generations is less than a predefined threshold value, which indicates that the population has converged to the PF of the unconstrained MOP or trapped into local optimization.

Then, the algorithm will switch to the second stage. In the pull stage, the feasible solution with the knee point will be pulled slowly to the real PF by using an improved epsilon constraint handling(IECH) mechanism, which is set as follows:

$$\varepsilon\left(k\right) = \begin{cases} \phi_\theta & \text{if} \quad k = 0 \\ (1-\tau)\varepsilon(k-1) & \text{if} rf_k < \alpha \\ \varepsilon\left(0\right)\left(1 - \dfrac{k}{T_c}\right)^{cp} & \text{if} rf_k \geqslant \alpha \\ 0 & \text{otherwise} \end{cases} \tag{32}$$

"where $\varepsilon(k)$ is the value of ε function, ϕ_θ means the overall constraint violation of the top θ-th individual in the initial population, rf_k refers to the proportion of feasible solutions in the generation k. τ controls the speed when the relaxation of constraints reduces in the case of $rf_k < \alpha$ ($\tau \in [0,1]$). α controls the searching preference between the feasible and infeasible regions. cp is employed to control the reducing interval of relaxation of constraints in the case of $rf_k \geqslant \alpha$. $\varepsilon(k)$ stops updating until the generation counter k reaches T_c. $\varepsilon(0)$ is set as the maximum overall constraint violation when the push search finishes (Fan et al., 2019a)".

3.4. An instantiation of PPS-KnEA

From the above discussion of knee points, it can be seen that it is very important to select knee points for evolution in the process of multi-

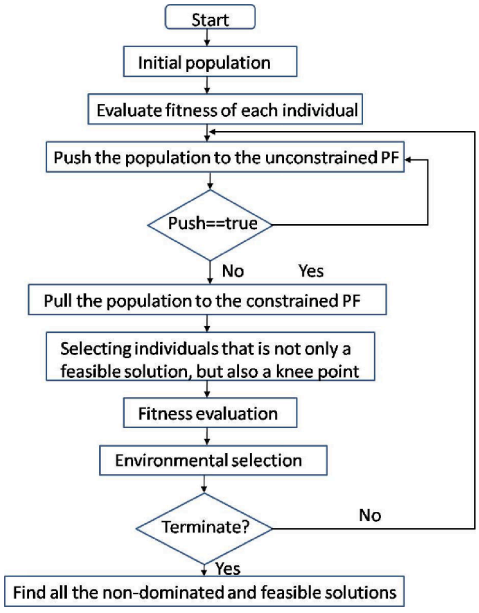

Fig. 5. General framework of the PPS-KnEA.

objective optimization. Nevertheless, the use of knee points to improve the search ability of CMOEA, especially for CMOPs that solve feasibility difficulties, has not been reported so far. In this work, we embed the Finding knee points method into the PPS framework to obtain a novel algorithm termed PPS-KnEA. In the PPS-KnEA algorithm, the knee points in the infeasible region can get across the infeasible region and converge to the PF with the help of PPS framework, and maintain the diversity of the population.

3.4.1. The general framework of the PPS-KnEA

The overall framework of the PPS-KnEA is illustrated in Fig.5. Firstly, the algorithm randomly generates an initial population with N individuals. Secondly, the PPS framework driven by knee points is applied to guide individuals to cross the infeasible area and converge to the real PF. Using the push search, the individual can quickly converge to the unconstrained PF, making the fitness value better and the individual with the knee point quickly converges to the unconstrained PF. Thirdly, in the pull search stage, the dynamic feasible individuals with knee point are pulled to the real PF under the improved epsilon constraint handling mechanism. To be detailed here, the strategy for finding knee points is to dynamically find the knee points in the small neighborhood of each individual. In other words, the local knee area is not exactly the knee point of the whole PF, so there will also be N individuals as the parent population of the next generation after environmental selection. Finally, individuals are selected through environment selection. Environment selection is to dynamically balance objective and constraints under the improved epsilon constraint handling (IECH) mechanism and select a more suitable solution for the next generation of individuals. Compared with PPS-MOEA/D, PPS-KnEA prefers knee points rather than just dynamic selection of feasible solutions. Algorithms 1 and Algorithms 2 give the main steps of environmental selection.

3.4.2. Analysis of PPS-KnEA

In order to analyze the effectiveness of the PPS-KnEA framework and understand its mechanism, it was combined with MOEA/D to solve the challenges of CMOP. The unconstrained Tchebycheff decomposition method is adopted in this paper, with the detailed definition of the decomposition function given as follows.

$$g^{te}\left(\mathbf{x},\lambda^i,z^*\right)=\max_{j=1,\ldots,m}\frac{1}{\lambda_j^i}\left(\left|f_j\left(\mathbf{x}\right)-z_j^*\right|\right) \tag{33}$$

where λ^i is a weight vector, and $\Sigma_{j=1,\ldots,m}\lambda_j^i=1,\lambda_j^i\geqslant 0$. z^* means the ideal point, and $z_j^*=\min_{k=1,\ldots,N}f_j(\mathbf{x}^k)$.

With the mentioned decomposition method, we decompose the MOP into a set of single optimization subproblems and optimize them simultaneously in a collaborative way. Each subproblem is associated with a decomposition function by using a weight vector λ^i, a set of N uniformly spread weight vectors $\lambda^1,\ldots,\lambda^N$ are adopted to formulate N subproblems. The weight vectors λ^i satisfy $\sum_{j=1}^m\lambda_j^i=1$ and $\lambda_j^i\geqslant 0$ for each $j\in\{1,\ldots,m\}$.

PPS-KnEA performs unconstrained search and constrained search under knee point driving. In the unconstrained search, MOP is decomposed into a set of unconstrained scalar subproblems. If the individual has the smaller value of g^{te}(Tchebycheff aggregation function) for the neighbors of ith subproblem, then the individual of the neighbor replaces the subproblem and searches for the local knee point information of unconstrained PF. It is worth noting that the individual on unconstrained PF is still an infeasible solution, because the constraint is not considered, so the information of the knee point is the knee point of the infeasible solution. In the process of constraint search, MOP is decomposed into a set of constrained scalar subproblems. The above four rules of IECH mechanism(Eq. 32) are used to update individuals driven by knee points. If a individual of the subproblem with the value of constraint violation less than zero, then the feasible solution which has smaller value of g^{te} for the neighbors of the subproblem will replace the individual of the subproblem. It should be noted that the constraint violation values here are dynamically controlled by the four laws of IECH mechanism, not real values of constraint violation, the $\varepsilon(k)$ of the IECH mechanism is the real values of constraint violation only when the individual is pushed to the real PF. If the individual constraint violation value of the subproblem is greater than zero, then the infeasible solution with the knee point and smaller value of g^{te} can replace the individual of the subproblem. Therefore, driven by knee points, more potential infeasible solutions can be found as the parent of the next generation, thus improving the diversity of the population.

In the push stage, the MOP is decomposed into a set of unconstrained scalar subproblems because the constraints are not considered. Algorithm 1 gives the pseudo-code of push search. In line 2–5, an individual was selected to survive in the next generation according to the value of g^{te}. The knee point is also pushed to an unconstrained PF without considering any constraints, so each solution has the information about knee point.

In the pull stage, the MOP is decomposed into a set of constrained scalar subproblems using the above decomposition method, these subproblems are collaborative optimized simultaneously under knee point driving. In Algorithm 2, in the process of updating the subproblem, an offspring replacing an individual of the population can be divided into three situations: two solutions x^j and y^j, if their global constraint violation is less than or equal to $\varepsilon(k)$, and the g^{te} of y^j is smaller than x^j, then x^j is replaced by y^j (line 2–5). If x^j and y^j have the same constraint violation value, x^j is replaced by y^j. If y^j is a knee point and the g^{te} of y^j is smaller than x^j (line 6–9). Otherwise, if the global constraint violation value of y^j is smaller than x^j and y^j is the knee point, then x^j is replaced by y^j (lines 10–12).

The pseudo-code of PPS-KnEA is introduced in Algorithm 3. In line 1–2, a CMOP is decomposed into N single-objective subproblems and these subproblems are initialized at line 2. Each subproblem is solved by employing a subpopulation. The algorithm runs repeatedly from line 3

to 40 until the termination condition is met. Seeing lines 4, if the distance from the solution to the extreme line or hyperplane is the greatest in its neighborhood, the solution is recognized as a knee point and placed in K. In lines 13–24, an improved epsilon constraint processing is used to set the value for epsilon in the push and pull phases. Lines 25–38 update the knee points of each subproblem while updating each subproblem. In line 27, when $r^2 \neq r^3$ is randomly selected, differential evolution (DE) is utilized to generate new solutions. When $r^2 = r^3$ is randomly selected, the knee points are selected from the neighborhoods of the subproblem for differential evolution to produce a new solution. Lines 16–29 show the transition between the push search phase and the pull search phase for each subproblem. When *push* = *true*, the algorithm automatically enters the unconstrained push stage, updates the knee points and sub-problem information while pushing, and converges to the unconstrained PF. When *pull* = *true*, the algorithm automatically enters the pull stage involving the epsilon constraint processing mechanism, and updates the knee points and sub-problem information while pulling. At line 41, a set of non-dominated and feasible solutions is output.

Algorithm 1. Push Subproblems

1 **Function** $result = PushSubproblems(\mathbf{x}^j, \mathbf{y}^i, z^*, F, K, T_r, r, t)$
2 **if** $g^{te}(\mathbf{y}^i|\lambda^i, z^*) \leq g^{te}(\mathbf{x}^j|\lambda^j, z^*)$ **then**
3 $\mathbf{x}^j = \mathbf{y}^i$
4 result=true
5 **end**
6 **return** $result$;
7 **end**

Algorithm 2. Pull Subproblems

1 **Function** $result = PullSubproblems(\mathbf{x}^j, \mathbf{y}^i, z^*, \varepsilon(k), F, K, T_r, r, t)$
2 **if** $\phi(\mathbf{y}^i) \leq \varepsilon(k)$ *and* $\phi(\mathbf{x}^j) \leq \varepsilon(k)$ **then**
3 **if** $g^{te}(\mathbf{y}^i|\lambda^i, z^*) \leq g^{te}(\mathbf{x}^j|\lambda^j, z^*)$ **then**
4 $\mathbf{x}^j = \mathbf{y}^i$; result=true
5 **end**
6 **else if** $\phi(\mathbf{y}^i) == \phi(\mathbf{x}^j)$ *and* $y^i \in K$ **then**
7 **if** $g^{te}(\mathbf{y}^i|\lambda^i, z^*) \leq g^{te}(\mathbf{x}^j|\lambda^j, z^*)$ **then**
8 $\mathbf{x}^j = \mathbf{y}^i$; result=true
9 **end**
10 **else if** $\phi(\mathbf{y}^i) < \phi(\mathbf{x}^j)$ *and* $y^i \in K$ **then**
11 $\mathbf{x}^j = \mathbf{y}^i$; result=true
12 **end**
13 **return** $result$;
14 **end**

Algorithm 3. PPS-KnEA

Algorithm 3: PPS-KnEA

Input:

N: the number of subproblems; N *Weight vectors* : λ^1,...,λ^N; T: the size of the neighborhood; δ: the probability of selection from neighbors; T_c: the control generation for $\varepsilon(k)$; n_r: the maximal number of solutions replaced by a child control generation for $\varepsilon(k)$; T_{max}: the maximum generation; r, t: adaptive parameters of kneepoint; K:set of knee points; T_r: rate of knee points in population.

Output: a set of non-dominated and feasible solutions.

Initialization:
Decompose a CMOP into N sub-populations associated with weight vectors. Generate a population $P = \{x^1, ..., x^N\}$randomly. for each $i = 1, ..., N$,set B(i)=$\{i_1, ..., i_T\}$, where λ^{i_1},...,λ^{i_T} are the T closest weight vectors to λ^i. Set the ideal point $z_j^* = min_{j=1,...,N} f_j(x^i)$; Set $T_r = 0.5, r = -1, t = -1$;
while *gen* $\leq T_{max}$ **do**
  $F \leftarrow$Nondominated-sort(P);
  Update r by formula (31)
  Calculate R by formula (30)
  Calculate the distance between each solution in F_i and L by formula (29)
  for *all* $P \in F_i$ **do**
    NB $\leftarrow \{a | a \in F_i \leftarrow |f_a^j - f_P^j| \leq R^j, 1 \leq j \leq M\}$
    $K \leftarrow K \bigcup \{P\}$
    $F_i \leftarrow F_i \setminus NB$
  end
  if $k >= l$ **then** Set $r_k = CalcMaxChange(k)$;
  if $k < T_c$ **then**
    if $r_k \leq \epsilon$ *and PushStage==true* **then**
      PushStage=false;
      $\varepsilon(k) = \varepsilon(0) = maxViolation$;
    else
      PushStage==false;
      Update $\varepsilon(k)$according to Eq.(33);
    end
  else
    $\varepsilon(k) = 0$;
  end
  for $i \leftarrow 1$ **to** N **do**
    if $rand < \delta$ **then** $S = B(i)$ **else** $s = \{1, ..., N\}$;
    Set $r^1 = i$ and select two indexes r^2 and r^3 from S randomly $r^2 \neq r^3$. Generate a new solution $\overline{y}$ from x^{r^1}, x^{r^2} by a DE operator.
    while $c \neq n_r$ *or* $S \neq \varnothing$ **do**
      select an element j from S randomly.
      if *Pushstage* $==$ *true* **then**
        result = PushSubproblems($\mathbf{x}^j$,$\mathbf{y}^i$,z^*, F, K)
      else
        result = PullSubproblems($\mathbf{x}^j$,$\mathbf{y}^i$,z^*,$\varepsilon(k), F, K$)
      end
      if *result* $==$ *true* **then** $c = c + 1$
      S=S\ $\{j\}$;
    end
  end
  k=k+1;
end
Find all the non-dominated and feasible solutions

3.5. Computational complexity of each tested CMOEA

MOEA/D decomposes the CMOP into N subproblems and uses Chebyshev method to sort each subproblem, so its total computational complexity is $O(MNT)$ (Zhang & Li, 2007), while NSGA-II directly non-dominant sorting all the populations, so its total computational complexity is $O(MN^2)$ (Deb et al., 2002). Where M is the number of objectives, N is the population size, and T is the size of the neighborhoods in MOEA/D-CDP. CM2M is a NSGA-II based algorithm, it decomposes a CMOP into k sub-regions and non-dominant sorting on each subregion. Therefore, the computational complexity of CM2M is only $1/K$ of NSGA-II, that is $O(KMS^2) = O(MN^2/K)$. Where S is the size of a subpopulation. PPS-MOEA/D and PPS-KnEA are MOEA/D based algorithms, therefore, the computational complexity of PPS-MOEA/D and PPS-KnEA are the same as that of MOEA/D-CDP.

4. Experimental study

To evaluate the performance of the proposed PPS-KnEA, and five other CMOEAs, including PPS-MOEA/D (Fan et al., 2019b), KnEA (Zhang et al., 2015), MOEA/D-CDP (Zhang & Li, 2007), NSGA-II-CDP (Deb et al., 2002), CM2M (Liu, Peng, Gu, & Wen, 2016a) are used to make comparisons. The detailed parameters are listed as follows:

1. The mutation probability $P_m = 1/n$ (n denotes the dimension of the decision vector). The distribution index in the polynomial mutation is set as 20.
2. Differential evolution(DE) parameters: $CR = 1.0, f = 0.5$.
3. Population size: $N = 300$. Neighborhood size: $T = 30$.
4. Halting condition: each algorithm runs for 30 times independently, and stops when 600,000 function evaluations are reached.
5. Probability of selecting individuals from its neighborhood: $\delta = 0.9$.
6. The max number of solutions updated by a child: $n_r = 2$.
7. Parameter setting in PPS-KnEA: $T_c = 1600, \alpha = 0.95, T = 0.05, cp = 2.\ l = 20$. The rate of knee points in population $Tr = 0.5$.
8. Parameter setting in PPS-MOEA/D: $T_c = 1600, \alpha = 0.95, T = 0.05, cp = 2.\ l = 20$.
9. Parameter setting in CM2M: $K = 10$.
10. Parameter setting in KnEA: $T_r = 0.5$.

4.1. Performance Metric

In order to evaluate the performance of the CMOEAs, two performance indicators, including the inverted generation distance (IGD) (Bosman & Thierens, 2003) and the hypervolume (HV) (Zitzler & Thiele, 1999), are adopted in this paper.

- **Inverted Generational Distance** (IGD):

Inverted Generational Distance(IGD) is an inverse mapping of Generational Distance(GD). It is expressed by the average distance from the individual in Pareto optimal solution set to the non-dominant solution set PF obtained by the algorithm. Therefore, the calculation formula is

$$\begin{cases} IGD\left(P^*, A\right) = \dfrac{\sum_{y^* \in P^*} d\left(y^*, A\right)}{|P^*|} \\ d\left(y^*, A\right) = \min_{y \in A}\left\{\sqrt{\sum_{i=1}^{m}\left(y_i^* - y_i\right)^2}\right\} \end{cases} \tag{34}$$

where P^* is a set of representative solutions in the true PF. $d(y^*, A)$ represents the minimum Euclidean distance from point y_i^* on the obtained Pareto optimal surface to individual y_i in P^*. The smaller the IGD value, represents that the population achieves the nondominated set closer to the true PF.

- **Hypervolume** (HV):

HV is a popular evaluation index, which reflects the closeness of the set of non-dominated solutions achieved by a CMOEA to the true PF. The performance of CMOEAs is evaluated by calculating the hypervolume of the space surrounded by the non-dominant solution set and the reference point. The calculation formula is as follows:

$$HV\left(S\right) = VOL\left(\bigcup_{x \in S}\left[f_1\left(x\right), z_1^r\right] \times \ldots \left[f_m\left(x\right), z_m^r\right]\right) \tag{35}$$

where $VOL(\cdot)$ is the Lebesgue measure, m means the number of objectives, $\mathbf{z}^r = (z_1^r, \ldots, z_m^r)^T$ refers to a user-defined reference point in the objective space. The larger the HV value, the better the performance of the algorithm. The reference point is placed at 1.2 times the distance to the nadir point of the true PF. A larger value of HV indicates better performance regarding diversity and convergence.

4.2. Experimental results

4.2.1. Performance comparisons

We conduct 30 independent runs for each CMOEA to solve the optimization problem of the TBM. The statistical results of IGD and HV values are listed in Table 4. Wilcoxon's rank sum test at a 0.05 significance level is performed between PPS-KnEA and each of the other five CMOEAs. † represents that the performance of the corresponding algorithm is significantly worse than that of PPS-KnEA. In terms of IGD and HV metric, the performance of PPS-KnEA is significantly better than those of PPS-MOEA/D, CM2M, MOEA/D-CDP, KnEA and NSGA-II-CDP on the optimization problem of the TBM.

The distributions of IGD and HV values for the six algorithms in the 30 independent runs are shown in Fig. 6. We can observe that PPS-KnEA has the highest median of IGD and HV value, which indicates that PPS-KnEA outperforms the other five algorithms in solving the performance optimization problem of the TBM.

From Table 4, we can obtain that PPS-KnEA performs significantly better than KnEA in terms of IGD and HV metrics, and PPS-MOEA/D is significantly better than MOEA/D-CDP in the IGD and HV metric. PPS-based methods (PPS-KnEA and PPS-MOEA/D) outperform their counterparts (KnEA and MOEA/D-CDP) without adopting PPS framework, which demonstrates the superiority of the PPS framework for solving the performance optimization of the TBM.

Non-dominated solutions achieved by each algorithm on the design

Table 4
The IGD and HV results of the six CMOEAs on the optimization problem of the TBM design.

Test Index		PPS-KnEA	CM2M	PPS-MOEA/D	MOEA/D-CDP	KnEA	NSGA-II-CDP
IGD	mean	**0.5661**	1.4126 †	0.5977†	1.0626†	76.4509†	101.2178†
	std	**0.0270**	0.1958†	0.0349 †	0.0679 †	37.153 †	50.0392†
HV	mean	**1.3942E + 07**	1.3891E + 07†	1.3940E + 07	1.3931E + 07 †	7.6983E + 06†	6.1869E + 06†
	std	**908.7283**	7.6141E + 03†	1.4043E + 03 †	2.1464E + 03 †	3.5457E + 06 †	3.7153E + 03†

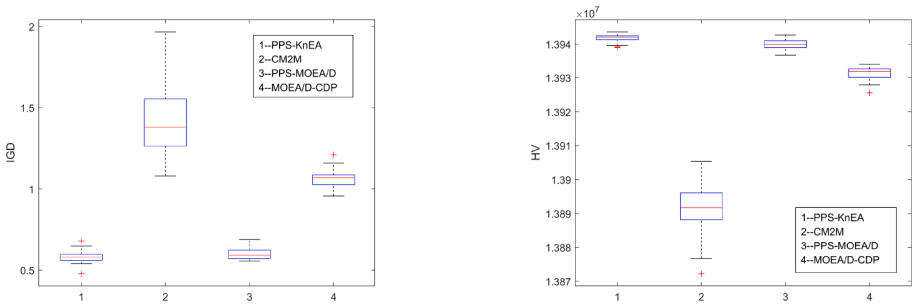

Fig. 6. The IGD box and HV box plot of PPS-KnEA and the other four CMOEAs on the optimization problem of the TBM design in 30 independent runs. To facilitate the display of the box plot, the number 1–4 represent PPS-KnEA, CM2M, PPS-MOEA/D, MOEA/D-CDP, respectively.

optimization of the TBM with the best HV values during the 30 independent runs are plotted in Fig. 7. It can be observed that most of the achieved solutions in PPS-KnEA are located in the reference PF, while the populations of the other five CMOEAs are trapped in local optima.

4.2.2. *Analysis of the results*

To study the characteristics of the TBM design optimization problem, 5, 200,000 solutions are generated as shown in Fig. 8, where 1,000,000 solutions are generated randomly, and the rest of the solutions are generated by PPS-KnEA, PPS-MOEA/D, CM2M, MOEA/D-CDP, KnEA and NSGA-II-CDP. The approximated landscape of the TBM optimization problem is a narrow strip. Some feasible and infeasible solutions are located in the same regions in the objective space. Its PF is hidden at the bottom of the infeasible region near the f1 axis, as shown in Fig. 8. Therefore, the TBM performance optimization problem is feasible-hard and converge-hard, which means it is difficult to get across the infeasible region and converge to the whole PF for a CMOEA.

Decomposition based CMOEAs decompose a CMOP into a set of single constrained optimization problems, which have an intrinsic capability to help the population get across the infeasible region. For example MOEA/D-CDP adopts the MOEA/D framework, while CM2M employs the NSGA-II framework in each sub-region, they are all decomposition based CMOEAs. Without the help of PPS, decomposition based CMOEAs such as MOEA/D-CDP and CM2M perform better than KnEA and NSGA-II-CDP, because the TBM performance optimization problem is feasible-hard and converge-hard, which can also be observed from Table 4.

Knee-points driven CMOEAs embed the Finding knee point method in the original framework, the knee points are used as a criterion only next to the dominance criterion in both mating and environmental selection, which can help the algorithm to maximize the hypervolume values, thus improving its diversity and convergence performance of the population. Knee points driven CMOEAs such as PPS-KnEA and KnEA perform better than PPS-MOEA/D and NSGA-II-CDP in terms of HV and IGD values, which can also be observed from Table 4. For PPS-KnEA embed the Finding knee points method in the PPS-MOEA/D framework, while KnEA embed the Finding knee points method in the NSGA-II framework, they are all knee points driven CMOEAs.

A characteristic of the TBM performance optimization problem is that the unconstrained PF is close to its constrained PF, it is almost part of unconstrained PF and in the infeasible region near the bottom of the f1 axis, and the ratio of feasible to infeasible solutions is small, as

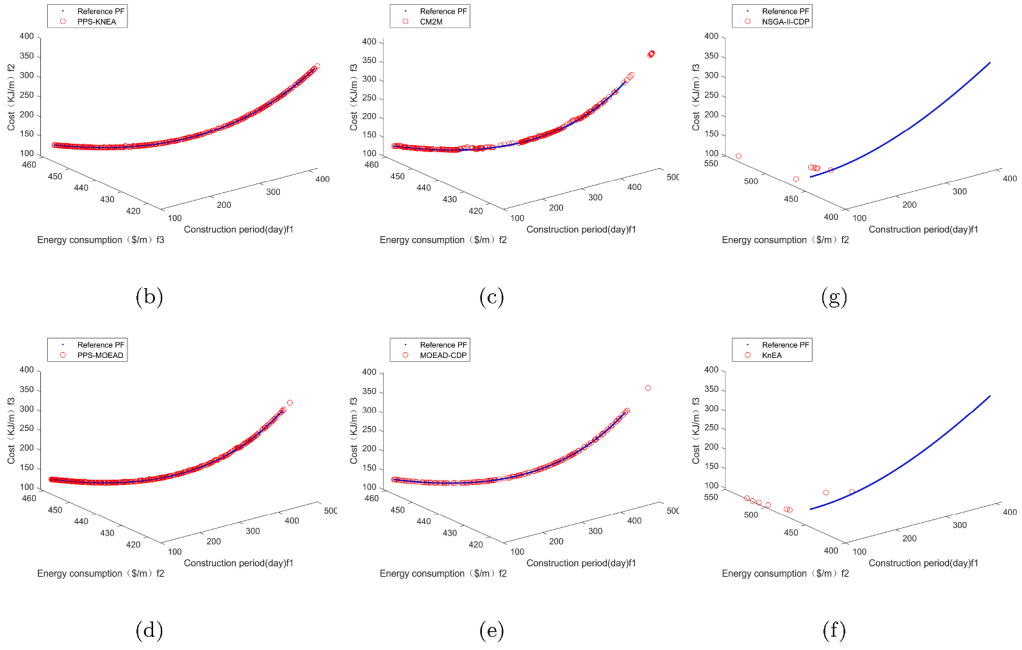

Fig. 7. Non-dominated solutions achieved by each algorithm on the design optimization of the TBM with the best HV values during the 30 independent runs are plotted.

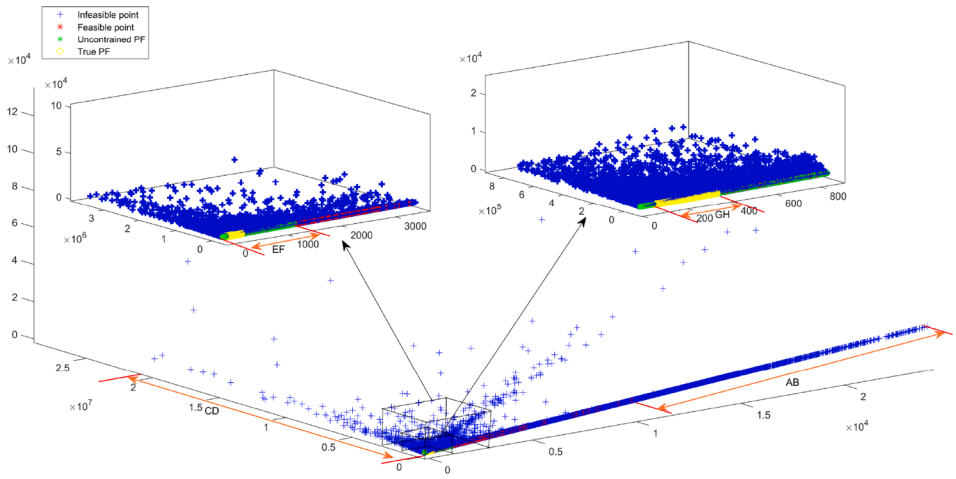

Fig. 8. The distribution of solutions of the TBM design optimization problem in the objective space.

illustrated by Fig. 8. To be more specific, AB and CD denote the distance between the infeasible regions and the reference PF. In the f1 and f2 axes, EF and GH denote the length of unconstrained PF and reference PF, as illustrated in Fig. 8. Since EF and GH are much smaller than AB and CD, it is easy for the PPS-based algorithms to pull the solutions across the infeasible regions from the unconstrained PF to the reference PF.

With the help of PPS framework, PPS-KnEA can search for knee points while crossing the infeasible region. This is the first time that the Finding knee point method have been used in PPS framework to increase the pressure of infeasible solution selection, so as to improve the diversity of the population. PPS-KnEA can fully consider the specific characteristics of TBM problem. Firstly, because constraints are not considered, many knee points are quickly pushed to the unconstrained PF. Secondly, because PPS-KnEA prefers knee points, the knee points in infeasible solutions are more favored than other infeasible solutions. The IECH mechanism can better balance the relationship among of the objectives, constraints and knee points, slowly pull the knee points in the population to the real PF, and then accelerate the convergence of the population.

Therefore, the integration of the Finding knee point method and PPS framework can not only help the population cross the infeasible region, but also improve the diversity of the population. PPS-KnEA performs better than other algorithms without Finding knee point method and PPS framework.

From the above discussion, we can conclude that PPS-KnEA outperforms the other five CMOEAs (PPS-MOEA/D, CM2M, MOEA/D-CDP, KnEA and NSGA-II-CDP) significantly on the TBM optimization problem. PPS-based methods (PPS-KnEA and PPS-MOEA/D) outperform their counterparts (KnEA and MOEA/D-CDP) without adopting PPS framework, which demonstrates the superiority of the PPS framework for solving the TBM design optimization problem. Methods using knee points (PPS-KNEA and KnEA) are superior to their counterparts (PPS-MOEA/D and NSGA-II-CDP) without Finding knee point method. This shows that under PPS framework, knee points driven algorithm can significantly improve the relevant evaluation indices (IGD and HV) of the algorithm in solving TBM problems.

4.2.3. Comparison with single objective optimization (SOP) algorithm

To our knowledge, this paper is the first time to optimize TBM using multi-objective optimization evolutionary algorithm. Its advantages are self-evident. A PS will be provided when an MOP is solved, while the SOP only has one solution. If an MOP is transformed into a SOP, the other two objectives in the MOP must be set as constraints. In order to fully illustrate the advantages of MOP, a state-of-the-art algorithm for SOP, particle swarm optimization (PSO), is employed as the comparing one. .

4.2.3.1. SOP model of TBM. Since it is an SOP, the optimization model of TBM must be readjusted. Only one of the three objectives will be selected as the optimization objective. Here, the construction period is selected as the optimization objective:

$$f = min(t) \tag{36}$$

The other two objectives, construction energy consumption and construction cost, are adjusted as constraints. According to the previous MOP results and engineering requirements, we control the construction energy consumption within 500 kJ/m and the construction cost within 400$/m.

$$500 - E \geqslant 0 \tag{37}$$

$$400 - C \geqslant 0 \tag{38}$$

The overall SOP model of TBM is provided as follows.

$$\begin{cases} \text{minimize} & \mathbf{F}(\mathbf{x}) = (t)^T \\ \text{subjectto} & 1.5 - \lambda \geqslant 0 \\ & 3000 - C_f \geqslant 0 \\ & 5 \times 10^6 - T_t \geqslant 0 \\ & 1.5 \times 10^7 - F_n \geqslant 0 \\ & 4.5 \times 10^6 - P_T \geqslant 0 \\ & 1.2 \times 10^4 - P_F \geqslant 0 \\ & 500 - E \geqslant 0 \\ & 400 - C \geqslant 0 \end{cases} \tag{39}$$

4.2.3.2. Introduction of PSO and experimental parameter setting. PSO algorithm was first developed by Kennedy and Eberhart (Kennedy & Eberhart, 1995). It is a swarm intelligence algorithm inspired by birds or fish. These swarms conform a cooperative way to find food, and each member in the swarms keeps changing the search pattern according to the learning experiences of its own and other members. The ith particle is represented as $X_i = (X_{i1}, X_{i2}, \ldots, X_{ip})$. The best previous position (the position giving the best fitness value) of the ith particle is recorded and represented as $P_i = (p_{i1}, p_{i2}, \ldots, p_{iD})$. The index of the best particle among all the particles in the population is represented by the symbol g. The rate of the position change (velocity) for particle i is represented as $V = (V_{i1}, V_{i2}, \ldots, V_{iD})$. The particles are manipulated according to the following equation: (Shi & Eberhart, 1999; Wang, Tan, & Liu, 2018)

$$V_{id} = W * V_{id} + c_1 * r_1 * \left(P_{id} - X_{id}\right) + c_2 * r_2 * \left(P_{gd} - X_{id}\right) \tag{40}$$

$$X_{id} = X_{id} + V_{id} \tag{41}$$

where $i = 1, 2, \ldots, N_P$, and N_P is the size of the population, c_1 and c_2 refer to the learning factors, and r_1 and r_2 mean two random numbers within

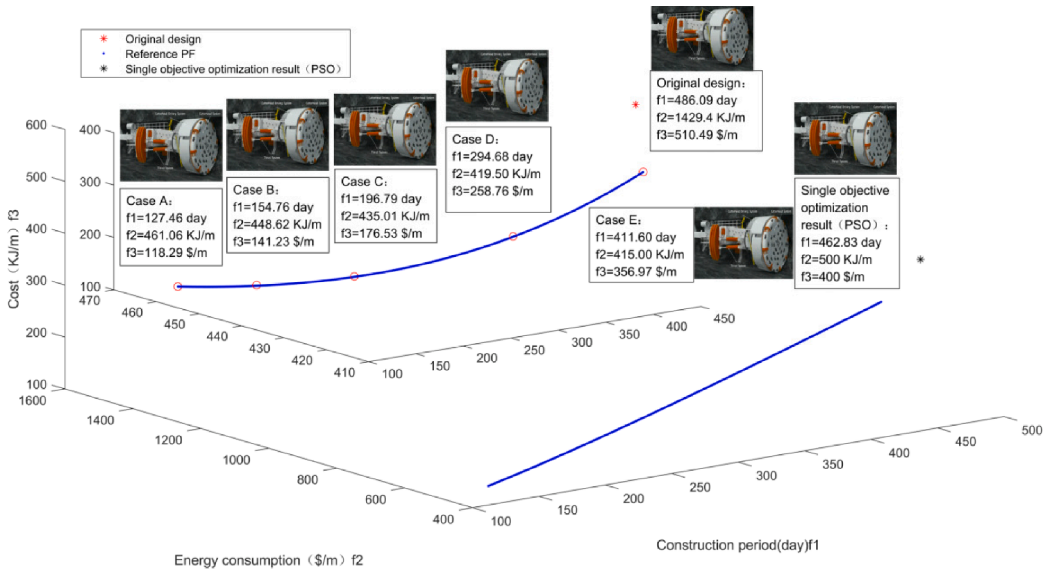

Fig. 9. The five points of the reference PF are selected as the representative cases to be compared with the original design by the human expert. The TBM models of the five solutions are drawn out with the different appearance to the original design and the single objective optimization result.zx

the range [0,1], W is the inertia weight. In order to help PSO solve constrained optimization problems, we embed Deb's (Deb et al., 2002) constraint dominance principle into PSO algorithm. The detailed parameters are listed as follows.

1. $c_1 = 2, c_2 = 2$.
2. The maximum number of iteration: $T_P = 500$.
3. Population size: $N_P = 300$.
4. $W = W_{Max} - 1 * ((W_{Max} - W_{Min})/T_P), W_{Max} = 0.9, W_{Min} = 0.2$.

4.2.3.3. Analysis and comparison of experimental results. As shown in Fig. 10, the relationship between construction period and Iteration obtained by SOP with PSO algorithm is presented. The minimum construction period optimized in the end is $t = 462.83$ (day), at which time the constraint violation value is zero, so the construction energy consumption is 500 (kJ/m) and the construction cost is 400 $/m. As shown in Fig. 9, the SOP results of PSO were dominated by PF of CMOEAs optimization results. Here, we can see that the SOP can only optimize the construction period, but the energy consumption and construction cost can only be set as constraints within a certain value. Meanwhile, the MOP can carry out collaborative optimization of multiple objectives, and finally find a group of PS.

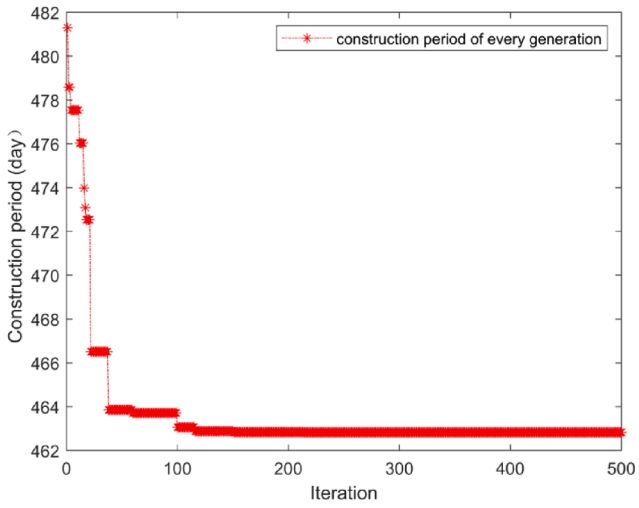

Fig. 10. Convergence histories of the Construction period and Iteration of the PSO.

4.2.4. The design of the TBM

The achieved reference PF obtained by six CMOEAs and the original design suggested by a human expert are shown in Fig. 8. Each solution in the reference PF dominates the original design. The performance of the TBM is improved significantly by using the proposed PPS-KnEA. Since the reference PF is a continuously convex PF, the endpoints and other three midpoints of the PF are selected as representative cases, as illustrated in Fig. 9. The detailed comparison of the original design by the human expert and the five representative solutions in the reference PF are listed in Table 5. The values of δ, H and α of case A, B, C, D, E are significantly change different from those values of $w, \omega$and r. A possible reason is that different constraints are activated in each different part of the reference PF.

4.2.5. Limitation of PPS

It is worth noting that PPS-based algorithms are not suitable for solving CMOPs whose unconstrained PFs are degenerated, which means the dimension of the unconstrained PFs is less than their constrained counterpart. One possible reason is that at the end of the push stage, the populations of PPS-based algorithms are converged to the unconstrained PFs. Since the unconstrained PFs are degenerated, the diversity of the populations in PPS-based algorithms is lost, and it is very difficult to pull the populations to the constrained PFs whose dimensions are greater than these of their unconstrained counterpart. Therefore, the PPS-KnEA algorithm which based on PPS also has the above limitation in solving practical constrained multi-objective optimization problems.

5. Conclution

In this paper, a hard rock TBM model is established and formulated as a constrained multi-objective optimization problem. Two kinds of PPS-based algorithms, including PPS-MOEA/D and PPS-KnEA, are employed to solve the formulated CMOP. It is worth noting that PPS-KnEA is a new algorithm which combines PPS with Finding knee point method to solve CMOPs. To be more specific, PPS-KnEA also divides the search process into two different stages push and pull search, as done in

Table 5
The decision variables, objective and constraint values of the five representative solutions and the original design.

	δ	ω	w	H	r	α	f_1	f_2	f_3	c_1	c_2	c_3	c_4	c_5	c_6
CaseA	11.06	10	2	0.86	100	31.86	127.46	461.06	118.29	1.06	13489634	2089940	2.13E-10	1452591.9	9.09E-13
CaseB	9.09	9.98	2	2.18	100	36	154.76	448.61	141.22	0.40	14269849	2669597	3324.17	2063431.6	5.22
CaseC	7.12	9.99	2	2.78	100.03	41.58	196.78	435.01	176.52	0.10	15097407	3229419	6177.58	2645965.8	4.11
CaseD	4.74	10	2	2.27	100	51.65	294.68	419.50	258.75	0.36	16157991	3862807	8962.67	3309134.2	1.83
CaseE	3.39	10	2	2.54	100	60.13	411.59	414.99	356.96	0.22	16789891	4195716	10186.38	3657755.5	9.09E-13
Original design	5	6	2	0.5	200	80	486.08	1429.4	510.48	1.16	829420	921700	1585.3	1937500	2730.9

PPS-MOEA/D. At the push search stage, a CMOP is decomposed into a set of simple constrained single-objective optimization problem and finding the knee points. Each simple constrained single-objective optimization problem corresponded to a sub-population with knee point information is solved by using MOEA/D without considering any constraints, which also can help each sub-population and its knee points get across infeasible regions efficiently. Some constrained information about the constrained landscape of the objective space will be gathered to help guide the parameters setting of the constraint processing mechanism in the pull search stage. At the beginning of the pull search stage, infeasible solutions in each subpopulation and knee points are pulled to the feasible and non-dominated regions by employing an improved epsilon constraint-handling mechanism and the knee points are used as a criterion only next to the dominance criterion in both mating and environmental selection.

The experimental results indicate that PPS-KnEA outperforms the other five CMOEAs (PPS-MOEA/D, CM2M, MOEA/D-CDP, KnEA and NSGA-II-CDP) significantly on the TBM optimization problem. PPS-based methods (PPS-KnEA and PPS-MOEA/D) outperform their counterparts (KnEA and MOEA/D) without adopting PPS framework, which demonstrates the superiority of the PPS framework for solving real-world optimization problems. Knee points driven methods (PPS-KnEA and KnEA) outperform their counterparts (PPS-MOEA/D and NSGA-II-CDP) without adopting Finding knee point method, which demonstrates that under the PPS framework, the knee points get across the infeasible region and evolve to a true PF. The selection of knee points is approximate to maximize the large hypervolume value, which helps accelerating population convergence and increasing diversity in solving the TBM problem.

It is notable that few works have been done by employing CMOEAs to solve real-world CMOPs. This paper provides a feasible method. In the future, we will study multi-scenario and multi-model optimization, and use different methods to model and optimize the overall performance of TBM, so as to test the performance of PPS based CMOEAs in solving real-world optimization problems.

Declaration of Competing Interest

The authors declare that they have no known competing financial interests or personal relationships that could have appeared to influence the work reported in this paper.

Acknowledgment

This work was jointly supported by the Key Lab of Digital Signal and Image Processing of Guangdong Province; by the Key Laboratory of Intelligent Manufacturing Technology (Shantou University), Ministry of Education; the Science and Technology Planning Project of Guangdong Province of China (180917144960530); the State Key Lab of Digital Manufacturing Equipment \& Technology (DMETKF2019020); the National Defense Technology Innovation Special Zone Projects; the Scientific Research Staring Foundation of Shantou University (NTF20009); the Natural Science Foundation of Guangdong Province of China (2021A1515011709); the Fundamental Research Funds for the Central Universities, JLU, (93K172021K13); the Natural Science Foundation of the Anhui Higher Education Institutions of China (KJ2019A0956); the Major Project of Natural Science Research of the Jiangsu Higher Education Institutions of China (21KJA520006); and the Xuzhou Science and Technology Plan Project (KC21007).

References

Armaghani, D. J., Faradonbeh, R. S., Momeni, E., Fahimifar, A., & Tahir, M. M. (2018). Performance prediction of tunnel boring machine through developing a gene expression programming equation. *Engineering With Computers, 34*, 129–141.
Armaghani, D. J., Koopialipoor, M., Marto, A., & Yagiz, S. (2019). Application of several optimization techniques for estimating TBM advance rate in granitic rocks. *Journal of rock mechanics and geotechnical engineering, 11*, 779–789.
Armaghani, D. J., Mohamad, E. T., Narayanasamy, M. S., Narita, N., & Yagiz, S. (2017). Development of hybrid intelligent models for predicting TBM penetration rate in hard rock condition. *Tunn. Undergr. Space Technol., 63*, 29–43.
Benardos, A., & Kaliampakos, D. (2004). Modelling TBM performance with artificial neural networks. *Tunn. Undergr. Space Technol., 19*, 597–605.
Bosman, P. A. N., & Thierens, D. (2003). The balance between proximity and diversity in multiobjective evolutionary algorithms. *IEEE Trans. Evol. Comput., 7*, 174–188.
Das, I. (1999). On characterizing the "knee" of the pareto curve based on normal-boundary intersection. *Structural optimization, 18*, 107–115.
Deb, K., Pratap, A., Agarwal, S., & Meyarivan, T. (2002). A fast and elitist multiobjective genetic algorithm: NSGA-II. *IEEE Trans. Evol. Comput., 6*, 182–197.
Fan, Z., Li, W., Cai, X., Li, H., Wei, C., Zhang, Q., Deb, K., & Goodman, E. (2019a). Difficulty adjustable and scalable constrained multi-objective test problem toolkit. *Evolutionary Computation*, 1–28. https://doi.org/10.1162/evco_a_00259
Fan, Z., Li, W., Cai, X., Li, H., Wei, C., Zhang, Q., Deb, K., & Goodman, E. (2019b). Push and pull search for solving constrained multi-objective optimization problems. *Swarm and Evolutionary Computation, 44*, 665–679.
Fan, Z., Wang, Z., Li, W., Yuan, Y., You, Y., Yang, Z., Sun, F., Ruan, J., & Li, Z. (2019c). Push and pull search embedded in an M2M framework for solving constrained multi-objective optimization problems. *Swarm and Evolutionary Computation, 54*, 100651.
Grima, M. A., Bruines, P., & Verhoef, P. (2000). Modeling tunnel boring machine performance by neuro-fuzzy methods. *Tunnelling and underground space technology, 15*, 259–269.
Home, L. (2016). Hard rock TBM tunneling in challenging ground: Developments and lessons learned from the field. *Tunn. Undergr. Space Technol., 57*, 27–32.
Kennedy, J., & Eberhart, R. (1995). Particle swarm optimization. In Proceedings of ICNN'95-international conference on neural networks (pp. 1942–1948). IEEE volume 4.
Liao, J., Chen, Z., & Yao, B. (2017). High-performance adaptive robust control with balanced torque allocation for the over-actuated cutter-head driving system in tunnel boring machine. *Mechatronics, 46*, 168–176.
Liu, H.-L., Peng, C., Gu, F., & Wen, J. (2016a). A constrained multi-objective evolutionary algorithm based on boundary search and archive. *Int. J. Pattern Recognit Artif Intell., 30*, 1659002.
Liu, Q., Huang, X., Gong, Q., Du, L., Pan, Y., & Liu, J. (2016b). Application and development of hard rock TBM and its prospect in china. *Tunn. Undergr. Space Technol., 57*, 33–46.
Ozdemir, L. (1977). Development of theoretical equations for predicting tunnel boreability. In *Ph.D. thesis Colorado School of Mines. Arthur Lakes Library*.
Qiu, J., Liu, M., Zhang, L., Li, W., & Cheng, F. (2019). A multi-level knee point based multi-objective evolutionary algorithm for auc maximization. *Memetic Computing, 11*, 285–296.
Rao, R. (2007). *Decision-Making in the Manufacturing Environment Using Graph Theory and Fuzzy Multiple Attribute Decision-Making Methods*. London: Springer-Verlag.
Rao, R., & Lakshmi, R. (2021a). R-method: A simple ranking method for multi-attribute decision-making in the industrial environment. *J. Project Manage, 6*, 1–8.
Rao, R., & Lakshmi, R. (2021b). Ranking of pareto-optimal solutions and selecting the best solution in multi- and many-objective optimization problems using R-method. *Soft Computing Letters, 3*, 100015.
Ren, D., Shen, S., Zhou, A., & Chai, J. (2018a). Prediction of lateral continuous wear of cutter ring in soft ground with quartz sand. *Comput. Geotech., 103*, 86–92.
Ren, D.-J., Shen, S.-L., Arulrajah, A., & Cheng, W.-C. (2018b). Prediction model of TBM disc cutter wear during tunnelling in heterogeneous ground. *Rock Mech. Rock Eng., 51*, 3599–3611.
Rostami, J. (1997). Development of a force estimation model for rock fragmentation with disc cutters through theoretical modeling and physical measurement of crushed zone pressure. In *Ph.D. thesis Colorado School of Mines Golden*.

Rostami, J. (2016). Performance prediction of hard rock tunnel boring machines (tbms) in difficult ground. *Tunn. Undergr. Space Technol., 57*, 173–182.
Rostami, J., & Ozdemir, L. (1993). A new model for performance prediction of hard rock TBMs. In *In Proceedings of the rapid excavation and tunneling conference* (pp. 793–809).
Rostami, P. E. J. (2008). Hard rock TBM cutterhead modeling for design and performance prediction. *Geomechanik Und Tunnelbau, 1*, 18–28.
Roxborough, F.F., & Phillips, H.R. (1975). Rock excavation by disc cutter. In International Journal of Rock Mechanics and Mining Sciences & Geomechanics Abstracts (pp. 361–366). volume 12.
Shi, Y., & Eberhart, R.C. (1999). Empirical study of particle swarm optimization. In Proceedings of the 1999 congress on evolutionary computation-CEC99 (Cat. No. 99TH8406) (pp. 1945–1950). IEEE volume 3.
Singh, P. M. (2014). Design and analysis of a micro tunnel boring machines TBM. *Universal Journal of Mechanical Engineering, 2*, 87–93.
Sun, W., Wang, X., Shi, M., Wang, Z., & Song, X. (2018). Multidisciplinary design optimization of hard rock tunnel boring machine using collaborative optimization. *Advances in Mechanical Engineering, 10*, 168781401875472.
Sun, W., Wang, X., Wang, L., Zhang, J., & Song, X. (2016). Multidisciplinary design optimization of tunnel boring machine considering both structure and control parameters under complex geological conditions. *Structural and Multidisciplinary Optimization, 54*, 1073–1092.
Tian, Y., Zhang, T., Xiao, J., Zhang, X., & Jin, Y. (2021). A coevolutionary framework for constrained multiobjective optimization problems. *IEEE Trans. Evol. Comput., 25*, 102–116.
Wang, D., Tan, D., & Liu, L. (2018). Particle swarm optimization algorithm: an overview. *Soft. Comput., 22*, 387–408.
Wang, H., & Wang, J. (2020). The multi-objective optimization of tunneling boring machine control based on geological conditions identification. *Journal of Intelligent Manufacturing and Special Equipment, 1*, 87–105.
Wang, L., Kang, Y., Zhao, X., & Zhang, Q. (2015). Disc cutter wear prediction for a hard rock TBM cutterhead based on energy analysis. *Tunn. Undergr. Space Technol., 50*, 324–333.
Wang, X., Yuan, Y., Mu, X., Sun, W., & Song, X. (2019). Sensitivity of TBM's performance to structural, control and geological parameters under different prediction models. *IEEE Access, 7*, 19738–19751.
Wijk, G. (1992). A model of tunnel boring machine performance. *Geotech. Geol. Eng., 10*, 19–40.
Yagiz, S. (2003). Development of rock fracture and brittleness indices to quantify the effects of rock mass features and toughness in the CSM model basic penetration for hard rock tunneling machines. In *Ph.D. thesis Colorado School of Mines Golden*.
Yagiz, S., & Karahan, H. (2011). Prediction of hard rock TBM penetration rate using particle swarm optimization. *Int. J. Rock Mech. Min. Sci., 48*, 427–433.
Yagiz, S., & Karahan, H. (2015). Application of various optimization techniques and comparison of their performances for predicting TBM penetration rate in rock mass. *Int. J. Rock Mech. Min. Sci., 80*, 308–315.
Yu, G., Jin, Y., & Olhofer, M. (2020). A multiobjective evolutionary algorithm for finding knee regions using two localized dominance relationships. *IEEE Trans. Evol. Comput., 25*, 145–158.
Zhang, Q., Huang, T., Huang, G., Cai, Z., & Kang, Y. (2013). Theoretical model for loads prediction on shield tunneling machine with consideration of soil-rock interbedded ground. *Science China-technological Sciences, 56*, 2259–2267.
Zhang, Q., & Li, H. (2007). MOEA/D: A multiobjective evolutionary algorithm based on decomposition. *IEEE Transactions on Evolutionary Computation, 11*, 712–731.
Zhang, X., Tian, Y., & Jin, Y. (2015). A knee point-driven evolutionary algorithm for many-objective optimization. *IEEE Transactions on Evolutionary Computation, 19*, 761–776.
Zitzler, E., & Thiele, L. (1999). Multiobjective evolutionary algorithms: A comparative case study and the strength pareto approach. *IEEE Transactions on Evolutionary Computation, 3*, 257–271.